

Geophysical Research Letters[®]












RESEARCH LETTER

10.1029/2023GL103136

Special Section:

The Large Marsquake of Sol 1222

Investigation of Martian Regional Crustal Structure Near the Dichotomy Using S1222a Surface-Wave Group Velocities

Zongbo Xu¹ , Adrien Broquet² , Nobuaki Fuji^{1,3} , Taichi Kawamura¹ , Philippe Lognonné^{1,3} , Jean-Paul Montagner^{1,3} , Lu Pan⁴, Martin Schimmel⁵ , Eléonore Stutzmann¹ , and William Bruce Banerdt⁶ 

Key Points:

- Joint inversion of the S1222a Rayleigh- and Love-wave group velocities provides 1D isotropic velocity models of the regional Martian crust
- These models indicate a high-velocity layer at ~7 km depth which could be due to the regional basaltic activity or the regional stress field
- Except for the high-velocity layer, these models are similar to the crustal structure beneath InSight lander from ~12 to 40 km depth

Supporting Information:

Supporting Information may be found in the online version of this article.

Correspondence to:

Z. Xu,
zongboxu@ipgp.fr

Citation:

Xu, Z., Broquet, A., Fuji, N., Kawamura, T., Lognonné, P., Montagner, J.-P., et al. (2023). Investigation of Martian regional crustal structure near the dichotomy using S1222a surface-wave group velocities. *Geophysical Research Letters*, 50, e2023GL103136. <https://doi.org/10.1029/2023GL103136>

Received 6 FEB 2023

Accepted 3 APR 2023

¹Université Paris Cité, Institut de physique du globe de Paris, CNRS, Paris, France, ²Lunar and Planetary Laboratory, University of Arizona, Tucson, AZ, USA, ³Institut universitaire de France, Paris, France, ⁴School of Earth and Space Sciences, University of Science and Technology of China, Hefei, China, ⁵Geosciences Barcelona-CSIC, Barcelona, Spain, ⁶Jet Propulsion Laboratory, California Institute of Technology, Pasadena, CA, USA

Abstract Knowledge of Martian crust and uppermost mantle aid us studying the planet's evolution. NASA's InSight mission provides seismic data being used to reveal the interior structure. Most studies have focused on the crustal structure beneath InSight lander, but the seismic structure of other regions has remained poorly known. We use surface-wave data to investigate the crustal structure of a large region along the Medusa Fossae Formation and the dichotomy. We adopt the largest-magnitude marsquake (S1222a) that has been recorded, which provides both Rayleigh- and Love-wave signals. We measure and jointly invert these surface-wave fundamental-mode group velocities from ~15 to 40 s to estimate the average 1D isotropic velocity models. These models includes a high-velocity layer at ~7-km depth, which could be due to a regional basaltic activity or regional stress. Our models also indicate that a common intra-crustal structure (~12–40 km depth) may exist in this region along the dichotomy.

Plain Language Summary NASA's Mars exploration mission, InSight, brought a seismometer module that recorded numerous marsquakes. These marsquake recordings reveal the crustal structure beneath the InSight lander. To study the crustal structure of other regions, one can utilize a type of seismic waves, the surface waves. The largest marsquake event observed during InSight provides surface-wave signals with a high signal-to-noise ratio. By analyzing these signals, we investigate the average crustal structure between the epicenter and the InSight landing site in a region near the equator and along the planet's dichotomy. We find a high-velocity layer at about 7 km depth compared to the layers above and below, which could be due to a regional flood basalt or the regional crustal compressional stress. Our result also exhibits the similar crustal structure (from around 12 to 40 km depth) as the structure beneath the InSight lander, which indicates the possibility of a similar intra-crustal structure existing along the Martian dichotomy.

1. Introduction

Investigation of Martian crustal and uppermost mantle structure is important for studying the planet's crustal geology and interior evolution. For example, studying the lithospheric structure beneath the Martian dichotomy may shed light on its origin. Before NASA's Interior Exploration using Seismic Investigations, Geodesy and Heat Transport (InSight) mission (Banerdt et al., 2020), measurements of the Martian gravity and topography were used to constrain the crustal structure (e.g., Nimmo & Stevenson, 2001; Zuber et al., 2000). The seismic observation conducted through InSight's seismometer (Lognonné et al., 2019) provided new insight into Martian seismicity and interior (e.g., Banerdt et al., 2020; Giardini et al., 2020; Lognonné et al., 2020). This revealed a first view of the subsurface/crustal structure at the InSight landing site (Lognonné et al., 2020), later improved using various methods such as ambient-vibration *H/V* (Hobiger et al., 2021), marsquake-coda *H/V* (Carrasco et al., 2022), compliance (Kenda et al., 2020; Onodera, 2022; Xu et al., 2022), receiver function (e.g., Kim et al., 2021; Knapmeyer-Endrun et al., 2021; Shi et al., 2022), and autocorrelation (e.g., Compaire et al., 2021; Deng & Levander, 2020; Schimmel et al., 2021).

Martian crustal structure varies globally. Knowledge of the seismically derived structure beneath the InSight lander is a point measure of the whole Martian crust and has been used as an important constraint on global crustal thickness models (e.g., Wieczorek et al., 2022). To investigate the crustal structures of regions away from the InSight landing site, one can utilize bouncing waves (Li, Beghein, McLennan, et al., 2022) and

© 2023 The Authors.

This is an open access article under the terms of the [Creative Commons Attribution-NonCommercial License](https://creativecommons.org/licenses/by-nc/4.0/), which permits use, distribution and reproduction in any medium, provided the original work is properly cited and is not used for commercial purposes.

surface waves. Surface waves can provide information of the crustal structure along the path from the quake epicenter to the seismic station (e.g., Spetzler et al., 2002; Zhou et al., 2004). In the InSight seismic catalog (InSight Marsquake Service, 2023), only three have shown convincing Rayleigh-wave signals: the S1222a marsquake and two large impacts S1000a and S1094b (Posiolova et al., 2022). The signals from the two impacts are from ~ 10 to 20 s in period, and the surface-wave paths of these two events are far away from the dichotomy (Kim et al., 2022b). The S1222a marsquake was detected after these two events and is the largest ($M_W^{M} 4.7$) seismic event ever recorded during InSight mission. This event provides both Love- and Rayleigh-wave signals (Kawamura et al., 2022). The S1222a surface-wave data can be observed in a wider frequency band (from ~ 15 to 40 s, Section 2) compared to the two previous Rayleigh-wave signals. Furthermore, the S1222a epicenter is estimated to be near the Martian dichotomy (Kawamura et al., 2022). Therefore, by utilizing the S1222a surface-wave data, we investigate the average crustal structure from the epicenter to the InSight lander (Figure 1a), which could aid us understanding the lithospheric structure beneath the dichotomy.

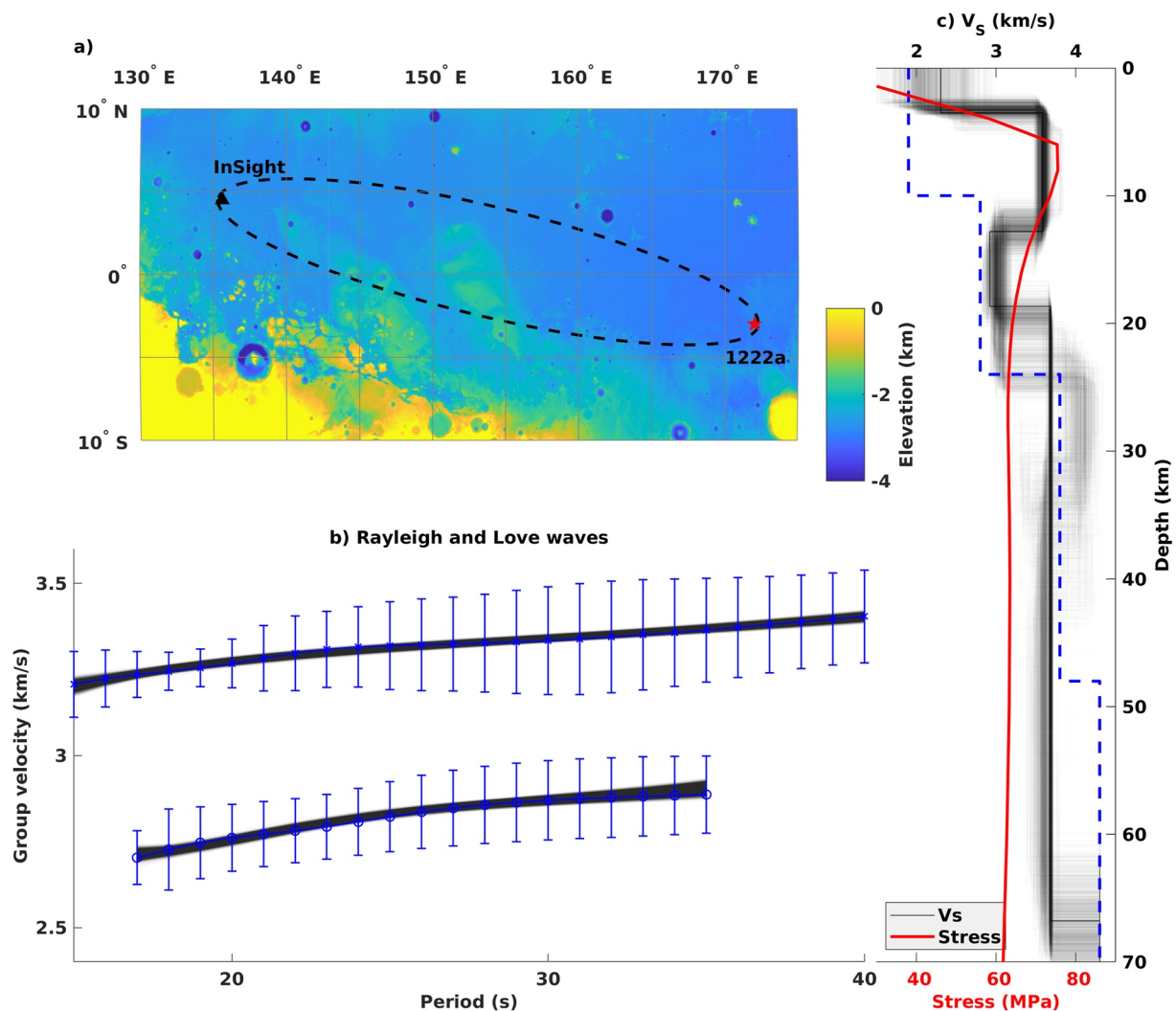


Figure 1. The map of the S1222a surface-wave sensitivity area on Martian ground surface and the inversion result of the surface-wave group-velocity measurements. We compute the sensitivity area (a) following Yoshizawa and Kennett (2005), and the details are in Section S1 and Figure S3 in Supporting Information S1. The upper and lower vertical bars (b) are the Love- and Rayleigh-wave group-velocity measurements, respectively. Each gray curve (b) is the synthetic Love-/Rayleigh-wave group velocity from the corresponding V_S model (gray lines in panel (c), Table S1 in Supporting Information S1 and Xu et al. (2023)), where the group-velocity forward modeling is from Herrmann (2013). The blue dashed line (c) is from Stähler et al. (2021) and is a characteristic V_S model of the crustal structure beneath the InSight lander (e.g., Knapmeyer-Endrun et al., 2021). The stress curve (c) is the averaged stress from 135° to 170°E and from -10° S to 10° N. The stress field estimate is from Broquet and Andrews-Hanna (2022) and represents the loading-induced regional stress field. Positive stress values mean compression.

Both Love and Rayleigh waves are sensitive to shear-wave velocity (V_s) structures (e.g., Aki & Richards, 2002), and the group/phase velocities can be used to estimate the crustal V_s models. Based on the assumption that the crust is isotropic, a joint inversion of both Rayleigh- and Love-wave group/phase velocities can be applied to estimate a V_s model (e.g., Aki, 1968; Brune & Dorman, 1963). However, one problem of the joint inversion is that 1D isotropic models may fail to explain both waves' dispersion curves (i.e., group/phase velocities) simultaneously (e.g., McEvelly, 1964; Shapiro et al., 2004). This phenomenon is called Rayleigh-Love discrepancy and could be due to the existence of anisotropic layers (e.g., Anderson, 1961) and/or thin isotropic layers (e.g., Backus, 1962), where the thickness of the thin layers is smaller compared to the wavelengths used in the inversion (e.g., Capdeville & Marigo, 2007).

In previous studies of the S1222a surface-wave data, Rayleigh-Love discrepancies were encountered and anisotropic models were adopted into the inversion (Beghein et al., 2022; Kim et al., 2022a). Here, instead of anisotropic models, we investigate if we could use isotropic thin-layer models to explain both the Rayleigh and Love wave dispersion curves (Section 3). The surface-wave wavelengths of S1222a are generally over 45 km (by assuming the phase velocity of 3 km/s). The Martian crust beneath the surface-wave sensitivity region is roughly from 30 to 40 km in thickness (Wieczorek et al., 2022) and the intra-crustal layers are thus even thinner compared to the wavelengths. Note that the goal of this study is not to distinguish which factor, anisotropy or thin layers, causes the discrepancy, because this is challenging even for terrestrial seismology (e.g., Alder et al., 2021; Fichtner et al., 2013; Wang et al., 2013). Here, we instead focus on the crustal structures from our inverted isotropic models and discuss the implications (Section 4).

2. S1222a Surface-Wave Data and Measurement

The S1222a epicenter is estimated to be about 37° away from the InSight landing site, and the back azimuth is $\sim 101^\circ$ (Kawamura et al., 2022). We remove the instrument response and the glitches from the S1222a raw data (e.g., InSight Mars SEIS Data Service, 2019a, 2019b; Scholz et al., 2020). We then rotate the north and east components to the radial and transverse components based on this event back azimuth (Figure 2). We bandpass filter these data between 10 and 100 s.

We observe the Rayleigh waves on the vertical and radial components (Figures 2a and 2c). These two component data indicate the retrograde-ellipse particle motion (Figures 2h and 2i), a classical property of fundamental-mode Rayleigh waves (e.g., Aki & Richards, 2002). The Love waves possess an almost linear particle motion along the transverse direction (Figures 2g, 2j, and 2m). We notice that in the transverse-radial plane, the dominant orientation of the Love- and Rayleigh-wave particle motions are tilted from the transverse and radial directions by an angle ($\sim 20^\circ$), respectively (Figures 2m–2o). Note that this angle is within the error bar of the back azimuth estimation (Kawamura et al., 2022). The origin of this angle is not clear yet, which may be due to the local anisotropy beneath the seismometer (e.g., Crampin, 1975; Li, Beghein, Wookey, et al., 2022) or to the lateral heterogeneities along the surface-wave propagation path (e.g., Kobayashi, 1998; Levshin et al., 1994). Further work on this angle is essential (e.g., Panning et al., 2023), as well as the Rayleigh-wave ellipse sloping (Figures 2h and 2i) and tilt (Figure 2l). For our study, we have checked that this angle does not affect our velocity measurements significantly.

We apply frequency-time analysis (e.g., Dziewonski et al., 1969) to the Rayleigh-wave vertical- and radial-component data to measure the group velocity. To avoid the source spectrum biasing the measurement (e.g., Cara, 1973), we adopt the correction proposed by Shapiro and Singh (1999). We plot the measurement results in the period-velocity domain (Figures S1a and S1b in Supporting Information S1). At each period, we pick the maximum as our group-velocity measurement, and we set the velocity difference between the group-velocity measurement and the maximum absolute values of the gradients around the measurement to be the uncertainty. From 17 to 35 s, the Rayleigh-wave group-velocity measurements from the vertical and radial components agree within the corresponding uncertainty at each period. Over 35 s, the Rayleigh-wave group-velocity differences between the two components are larger than the uncertainties. This could be due to the Rayleigh-wave signal amplitudes becoming comparable to the noise in the periods over 35 s (Figures 2b and 2d). Below 17 s, the trends in the Rayleigh-wave group-velocity measurements do not converge (Figures S1a and S1b in Supporting Information S1). Thus we use the Rayleigh-wave group-velocity measurements between 17 and 35 s for the following inversion.

Following the same processing, we measure the Love-wave group velocity between 15 and 40 s, where the Love-wave amplitude is larger than the noise (Figure 2f). The measurement indicates a divergence at 15 s (Figure S1c

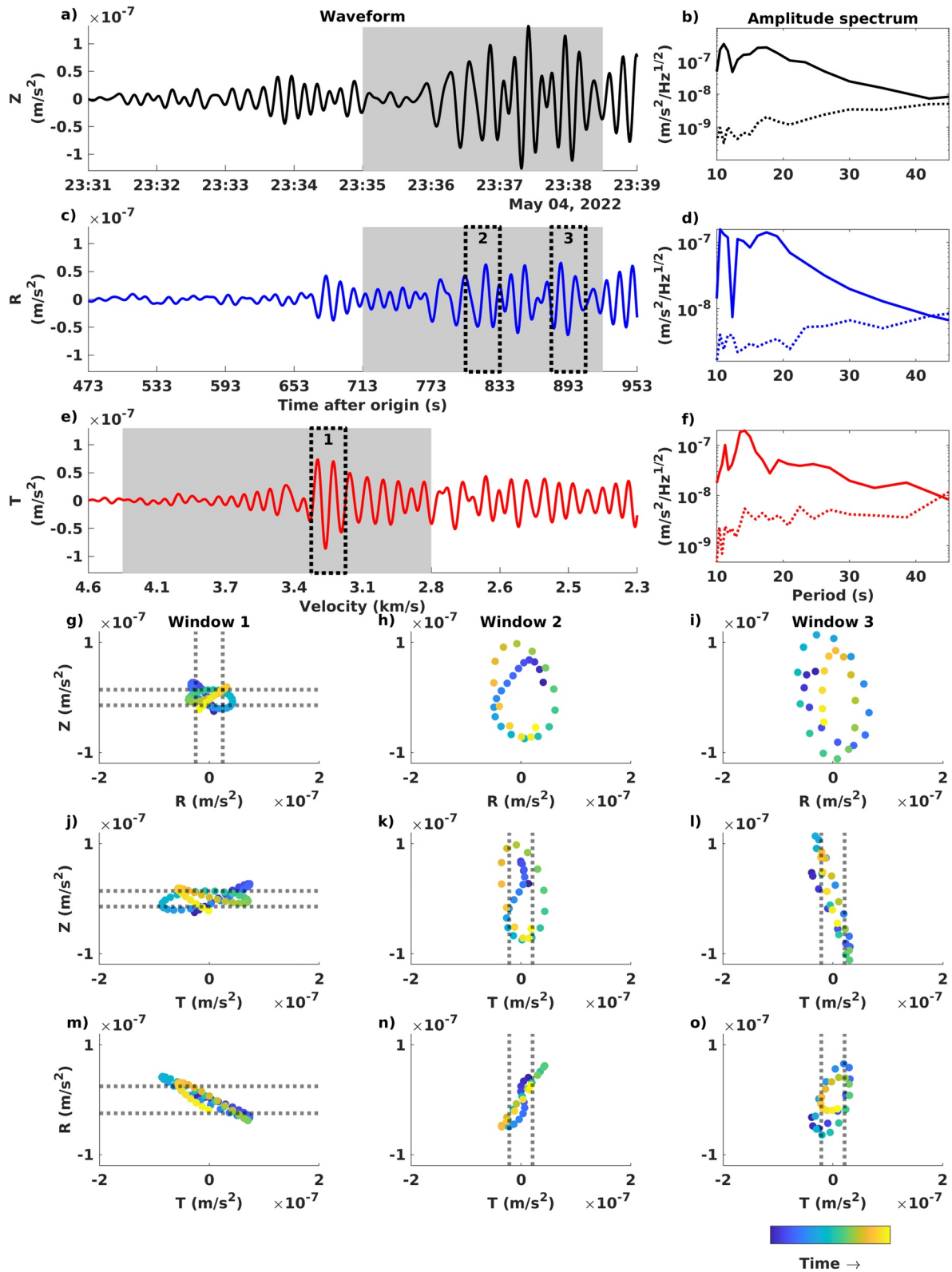


Figure 2.

in Supporting Information S1); indeed, in the time domain, the waveforms with periods ~ 15 s still exist after the Love-wave time window (Figure 2e). Thus, to avoid this ringing, we do not pick the short-period (< 15 s) Love-wave group velocities. Note that both our Rayleigh- and Love-wave group-velocity measurements agree well with the measurements from Beghein et al. (2022) between ~ 15 and 35 s (Figure S2 in Supporting Information S1).

3. Inversion Method and Results

We apply trans-dimensional Markov-chain Monte Carlo inversion to our surface-wave group-velocity measurements. To implement the inversion, we make use of the BayHunter (Dreiling & Tilmann, 2019) open-source inversion package. This package is developed for 1D isotropic velocity models, and the forward modeling module is from Computer Programs in Seismology (Herrmann, 2013). For each model, the package allows the number of layers, the V_s of each layer, and the layer thickness to evolve iteratively. We set the minimum layer thickness to be 2 km, as Shi et al. (2022) report a ~ 2 -km-thickness layer beneath the InSight lander. We set one V_p/V_s ratio for each model, and this ratio is allowed to vary between 1.70 and 1.85 during the inversion. The density of each layer is determined by the V_p -density relationship proposed by Berteussen (1977). We focus on the velocity model of the upper 70 km depth range because the surface-wave sensitivities are almost zero beneath this depth (Section S2 and Figure S4 in Supporting Information S1). We set the model parameters (i.e., V_p , V_s , and density) beneath 70 km to be the same as the parameters at the same depth from Stähler et al. (2021), assuming the Martian mantle beneath 70 km depth is laterally homogeneous.

We simultaneously invert the observed Rayleigh- and Love-wave group velocities. We restrict the first layer to possessing V_s lower than 3 km/s, because the surface-wave sensitivity region overlaps with Medusae Fossae Formation (MFF) which possesses low densities (e.g., Ojha & Lewis, 2018). We notice that beneath the first layer, our velocity models exhibit a high-velocity layer at ~ 7 km depth (Figure 1c); we discuss the origin of this layer in Section 4. The third layer (from ~ 12 to 20 km depth), which is beneath this high-velocity layer, possesses ~ 3 km/s V_s (Figure 1c), similar to the structure in this same depth range beneath the InSight lander (e.g., Knapmeyer-Endrun et al., 2021). At ~ 20 km depth, our V_s models present a velocity contrast, consistent with the previous study using the S1222a Rayleigh-wave data (Li, Beghein, Lognonné, et al., 2022). This velocity contrast also corresponds well with the interface at ~ 20 km depth beneath the InSight lander (e.g., Compaire et al., 2021; Knapmeyer-Endrun et al., 2021; Schimmel et al., 2021) and could be due to a pore closure process beneath that depth (e.g., Gyalay et al., 2020; Li, Beghein, McLennan, et al., 2022).

Beneath the velocity contrast, our velocity models agree with the previous studies about the crustal structure beneath the InSight lander (e.g., Durán et al., 2022; Knapmeyer-Endrun et al., 2021; Stähler et al., 2021) until the crust-mantle interface (from ~ 40 to 50 km depth) reported before. The absence of this interface in the regions away from the InSight landing site has been reported and is interpreted as the thicker crust in the these regions than beneath the InSight lander (Kim et al., 2021, 2022a; Li, Beghein, McLennan, et al., 2022).

4. Discussion and Conclusion

Our inversion provides the isotropic velocity models satisfying our Rayleigh- and Love-wave group velocity measurements within the uncertainties. These models share a similar structure (from ~ 12 to 40 km depth) as the crust beneath the InSight lander, indicating that this structure may exist regionally along the dichotomy.

The high-velocity layer from ~ 3 to 12 km depth in our models has not been observed before in the crustal structure beneath the InSight lander (e.g., Knapmeyer-Endrun et al., 2021). This high-velocity layer could be due to a rigid layer (e.g., a regional flood basalt during the Hesperian period, even late Noachian). The region between InSight and the epicenter of S1222a (Figure 1a) is mostly covered by the MFF unit. This unit overlies the adjacent early Hesperian transition unit (Tanaka et al., 2014) which is the same unit as beneath the lander. One possibility

Figure 2. S1222a Rayleigh and Love waveforms on the vertical (Z), radial (R), and transverse (T) components. The positive Z direction is pointing up and the positive R direction is in the great circle path from the epicenter to the InSight lander. The three component data are bandpass-filtered between 10 and 100 s in period (a, c, and e). The x-axes of the three subplots are in the same UTC time, and we convert the UTC time (a) to the time after the source origin (c) and the corresponding group velocity (e). The gray areas in panel (a) (or c) and (e) indicate the Rayleigh- and Love-wave time windows, respectively. For each component, we plot the amplitude spectra of the corresponding time window in solid lines (b, d, and f), and we also plot the noise amplitude spectra in dashed lines. The noise at each component is the mean of three time windows before the P arrival, and the time window length is the same as the data time window of each component. We also plot the particle motion in three short time windows (from (g) to (o)). The dashed lines at each time window are the standard deviation of the corresponding component data.

is that the emplacement of the MFF unit protected the underlying rigid layer from intense impact fracturing, while the medium beneath the InSight landing area was exposed to more recent impacts and thus possesses a higher porosity (e.g., Raducan et al., 2020). The low density MFF unit overlying the subsurface unit may have strengthened the velocity contrast at 2–3 km depth. To validate this hypothesis, we need simulation of impact fracturing the crustal media with and without a porous surface layer to better understand how the crustal fractures/porosity varies with depth between these two scenarios.

Another possible explanation for the high-velocity layer is related to the porosity varying with the regional stress field. We compare our V_S models to the stress state in the surface-wave sensitivity region (Figure 1c). The stress estimate is from Broquet and Andrews-Hanna (2022) and represents the integrated history of ancient loading, brittle failure, and recent plume-induced uplift at Elysium Planitia. We notice that this high-velocity layer (from 3 to 12 km) agrees well with the compressional stress peak at ~ 7 km depth. Since the crustal material within the first 20 km is preferred to be fractured (e.g., Kilburn et al., 2022), the compressional stress peak indicates that the materials around the peak depth may possess a lower porosity and thus a higher velocity than the upper and lower layers (e.g., Manga & Wright, 2021). Note that our velocity models are derived from the surface-wave data and thus represent an averaged structure in the surface-wave sensitivity region (Figure 1). This could explain why the previous studies do not observe this high-velocity layer, because these studies reveal a point measurement (i.e., the InSight landing site), where the local crustal porosity could be modified by the local stress or the nearby impacts (e.g., Gyalay & Nimmo, 2022). Validation of this hypothesis requires quantitative estimation of the porosity changes due to the regional stress. Given the two possibilities and lack of the validations, we cannot determine which possibility is preferred.

Meanwhile, because this high-velocity-layer thickness (~ 9 km) is about a fifth of the minimum surface-wave wavelength (~ 45 km) used in this study, our isotropic models can be homogenized to radial anisotropic models (e.g., Backus, 1962; Capdeville & Marigo, 2007). Application of the homogenization to our models indicates $(V_{SH}/V_{SV})^2 > 1$ (Figure S5 in Supporting Information S1), agreeing with Beghein et al. (2022) which interpreted that the radial anisotropy of $(V_{SH}/V_{SV})^2 > 1$ exists between 10 and 25 km depth using the same event. However, compared to the anisotropic estimate from Beghein et al. (2022), our homogenization presents lower $(V_{SH}/V_{SV})^2$ ratios (Figure S5 in Supporting Information S1). Thus, further investigation of the crustal structure in this region is required to determine if the structure is isotropic-layered or anisotropic and which geological activity may have led to this structure.

Data Availability Statement

The Martian topography data are from the NASA PDS Geosciences Node (Neumann et al., 2003). The InSight seismic waveform data are available from the IGP Datacenter, IRIS-DMC and the NASA PDS (InSight Mars SEIS Data Service, 2019a, 2019b) and secondary data of S1222a (e.g., location, arrival times) is available from MQS catalog (InSight Marsquake Service, 2023). The inversion package, BayHunter, is from Dreiling and Tilmann (2019). The velocity models from the inversion are available from Xu et al. (2023). The direct solution method (Geller & Ohminato, 1994) used in the Supporting Information S1 is from Fuji et al. (2016).

References

- Aki, K. (1968). Seismological evidences for the existence of soft thin layers in the upper mantle under Japan. *Journal of Geophysical Research*, 73(2), 585–594. <https://doi.org/10.1029/jb073i002p00585>
- Aki, K., & Richards, P. G. (2002). Quantitative seismology.
- Alder, C., Debayle, E., Bodin, T., Paul, A., Stehly, L., Pedersen, H., & Group, A. W. (2021). Evidence for radial anisotropy in the lower crust of the Apennines from Bayesian ambient noise tomography in Europe. *Geophysical Journal International*, 226(2), 941–967. <https://doi.org/10.1093/gji/ggab066>
- Anderson, D. L. (1961). Elastic wave propagation in layered anisotropic media. *Journal of Geophysical Research*, 66(9), 2953–2963. <https://doi.org/10.1029/jz066i009p02953>
- Backus, G. E. (1962). Long-wave elastic anisotropy produced by horizontal layering. *Journal of Geophysical Research*, 67(11), 4427–4440. <https://doi.org/10.1029/jz067i011p04427>
- Banerdt, W. B., Smrekar, S. E., Banfield, D., Giardini, D., Golombek, M., Johnson, C. L., et al. (2020). Initial results from the InSight mission on Mars. *Nature Geoscience*, 13(3), 183–189. <https://doi.org/10.1038/s41561-020-0544-y>
- Beghein, C., Li, J., Weidner, E., Maguire, R., Wookey, J., Lekić, V., et al. (2022). Crustal Anisotropy in the Martian lowlands from surface waves. *Geophysical Research Letters*, 49(24), e2022GL101508. <https://doi.org/10.1029/2022gl101508>
- Berteussen, K.-A. (1977). Moho depth determinations based on spectral-ratio analysis of NORSAR long-period P waves. *Physics of the Earth and Planetary Interiors*, 15(1), 13–27. [https://doi.org/10.1016/0031-9201\(77\)90006-1](https://doi.org/10.1016/0031-9201(77)90006-1)

Acknowledgments

The authors acknowledge the NASA, the CNES, their partner agencies and Institutions (UKSA, SSO, DLR, JPL, IGP-CNRS, ETHZ, IC, and MPS-MPG) and the flight operations team at JPL, SISMOC, MSDS, IRIS-DMC, and PDS for providing the SEED SEIS data. Z.X. thanks Mark Wieczorek for fruitful discussion. The authors thank Caroline Beghein for providing their surface-wave group-velocity measurements. The authors also thank Yann Capdeville for sharing the homogenization package. The authors thank editor Andrew Dombard and one anonymous reviewer for their constructive feedback that helped improve this manuscript. This research is supported by CNES, ANR MAGIS (ANR-19-CE31-0008-08), and the Initiative d'Excellence (IdEx) Université Paris Cité (ANR-18-IDEX-0001). This study is InSight contribution number 276.

- Broquet, A., & Andrews-Hanna, J. (2022). Geophysical evidence for an active mantle plume underneath Elysium Planitia on Mars. *Nature Astronomy*, 7(2), 160–169. <https://doi.org/10.1038/s41550-022-01836-3>
- Brune, J., & Dorman, J. (1963). Seismic waves and Earth structure in the Canadian shield. *Bulletin of the Seismological Society of America*, 53(1), 167–209.
- Capdeville, Y., & Marigo, J.-J. (2007). Second order homogenization of the elastic wave equation for non-periodic layered media. *Geophysical Journal International*, 170(2), 823–838. <https://doi.org/10.1111/j.1365-246x.2007.03462.x>
- Cara, M. (1973). Filtering of dispersed wavetrains. *Geophysical Journal International*, 33(1), 65–80. <https://doi.org/10.1111/j.1365-246x.1973.tb03415.x>
- Carrasco, S., Knapmeyer-Endrun, B., Margerin, L., Schmelzbach, C., Onodera, K., Pan, L., et al. (2022). Empirical H/V spectral ratios at the InSight landing site and implications for the Martian subsurface structure. *Geophysical Journal International*, 232(2), 1293–1310. <https://doi.org/10.1093/gji/ggac391>
- Compaire, N., Margerin, L., Garcia, R. F., Pinot, B., Calvet, M., Orhand-Mainsant, G., et al. (2021). Autocorrelation of the ground vibrations recorded by the SEIS-InSight seismometer on Mars. *Journal of Geophysical Research: Planets*, 126(4), e2020JE006498. <https://doi.org/10.1029/2020je006498>
- Crampin, S. (1975). Distinctive particle motion of surface waves as a diagnostic of anisotropic layering. *Geophysical Journal International*, 40(2), 177–186. <https://doi.org/10.1111/j.1365-246x.1975.tb07045.x>
- Deng, S., & Levander, A. (2020). Autocorrelation reflectivity of Mars. *Geophysical Research Letters*, 47(16), e2020GL089630. <https://doi.org/10.1029/2020gl089630>
- Dreiling, J., & Tilmann, F. (2019). BayHunter-McMc transdimensional Bayesian inversion of receiver functions and surface wave dispersion. [Software]. GFZ Data Services. <https://doi.org/10.5880/GFZ.2.4.2019.001>
- Durán, C., Khan, A., Ceylan, S., Zenhäuser, G., Stähler, S., Clinton, J., & Giardini, D. (2022). Seismology on Mars: An analysis of direct, reflected, and converted seismic body waves with implications for interior structure. *Physics of the Earth and Planetary Interiors*, 325, 106851. <https://doi.org/10.1016/j.pepi.2022.106851>
- Dziewonski, A., Bloch, S., & Landisman, M. (1969). A technique for the analysis of transient seismic signals. *Bulletin of the Seismological Society of America*, 59(1), 427–444. <https://doi.org/10.1785/bssa0590010427>
- Fichtner, A., Kennett, B. L., & Trampert, J. (2013). Separating intrinsic and apparent anisotropy. *Physics of the Earth and Planetary Interiors*, 219, 11–20. <https://doi.org/10.1016/j.pepi.2013.03.006>
- Fuji, N., Meschede, M., Konishi, K., Jaegler, H., Kawai, K., Zhao, L., et al. (2016). DSM kernel suite. Retrieved from <https://fpgp.github.io/DSM-Kernel/>
- Geller, R. J., & Ohminato, T. (1994). Computation of synthetic seismograms and their partial derivatives for heterogeneous media with arbitrary natural boundary conditions using the direct solution method. *Geophysical Journal International*, 116(2), 421–446. <https://doi.org/10.1111/j.1365-246x.1994.tb01807.x>
- Giardini, D., Lognonné, P., Banerdt, W. B., Pike, W. T., Christensen, U., Ceylan, S., et al. (2020). The seismicity of Mars. *Nature Geoscience*, 13(3), 205–212. <https://doi.org/10.1038/s41561-020-0539-8>
- Gyalay, S., & Nimmo, F. (2022). Closing pores and cracking: A window to Martian history from a seismic wave speed discontinuity in the crust. In *53rd Lunar and Planetary Science Conference*, (Vol. 2678, p. 1633). Retrieved from <https://ui.adsabs.harvard.edu/abs/2022LPLCo2678.1633G>
- Gyalay, S., Nimmo, F., Plesa, A.-C., & Wiczeorek, M. (2020). Constraints on thermal history of Mars from depth of pore closure below InSight. *Geophysical Research Letters*, 47(16), e2020GL088653. <https://doi.org/10.1029/2020gl088653>
- Herrmann, R. B. (2013). Computer programs in seismology: An evolving tool for instruction and research. *Seismological Research Letters*, 84(6), 1081–1088. <https://doi.org/10.1785/0220110096>
- Hobiger, M., Hallo, M., Schmelzbach, C., Stähler, S., Fäh, D., Giardini, D., et al. (2021). The shallow structure of Mars at the InSight landing site from inversion of ambient vibrations. *Nature Communications*, 12(1), 1–13. <https://doi.org/10.1038/s41467-021-26957-7>
- InSight Marsquake Service. (2023). *Mars seismic catalogue, InSight mission; V13 2023-01-01*. ETHZ, IPGP, JPL, ICL, Univ. Bristol. <https://doi.org/10.12686/a19>
- InSight Mars SEIS Data Service. (2019a). Data Service, InSight SEIS data bundle. *PDS Geosciences (GEO) Node*. <https://doi.org/10.17189/1517570>
- InSight Mars SEIS Data Service. (2019b). *SEIS raw data, InSight mission*. IPGP, JPL, CNES, ETHZ, ICL, MPS, ISAE-Supaero, LPG, MFSC. https://doi.org/10.18715/SEIS.INSIGHT.XB_2016
- Kawamura, T., Clinton, J. F., Zenhäuser, G., Ceylan, S., Horleston, A. C., Dahmen, N. L., et al. (2022). S1222a—the largest Marsquake detected by InSight. *Geophysical Research Letters*, 50(5), e2022GL101543. <https://doi.org/10.1029/2022GL101543>
- Kenda, B., Drilleau, M., Garcia, R. F., Kawamura, T., Murdoch, N., Compaire, N., et al. (2020). Subsurface structure at the InSight landing site from compliance measurements by seismic and meteorological experiments. *Journal of Geophysical Research: Planets*, 125(6), e2020JE006387. <https://doi.org/10.1029/2020je006387>
- Kilburn, R., Dasent, J., Wright, V., & Manga, M. (2022). Lithology, pore-filling media, and pore closure depth beneath InSight on Mars inferred from shear wave velocities. *Journal of Geophysical Research: Planets*, 127(12), e2022JE007539. <https://doi.org/10.1029/2022je007539>
- Kim, D., Banerdt, W., Ceylan, S., Giardini, D., Lekić, V., Lognonné, P., et al. (2022a). Structure along the Martian dichotomy constrained by Rayleigh and love waves and their overtones. *Geophysical Research Letters*, e2022GL101666. <https://doi.org/10.1029/2022GL101666>
- Kim, D., Banerdt, W., Ceylan, S., Giardini, D., Lekić, V., Lognonné, P., et al. (2022b). Surface waves and crustal structure on Mars. *Science*, 378(6618), 417–421. <https://doi.org/10.1126/science.abq7157>
- Kim, D., Lekić, V., Irving, J. C., Schmerr, N., Knapmeyer-Endrun, B., Joshi, R., et al. (2021). Improving constraints on planetary interiors with PPS receiver functions. *Journal of Geophysical Research: Planets*, 126(11), e2021JE006983. <https://doi.org/10.1029/2021je006983>
- Knapmeyer-Endrun, B., Panning, M. P., Bissig, F., Joshi, R., Khan, A., Kim, D., et al. (2021). Thickness and structure of the Martian crust from InSight seismic data. *Science*, 373(6553), 438–443. <https://doi.org/10.1126/science.abf8966>
- Kobayashi, R. (1998). Polarization anomaly of love waves caused by lateral heterogeneity. *Geophysical Journal International*, 135(3), 893–897. <https://doi.org/10.1046/j.1365-246x.1998.00702.x>
- Levshin, A. L., Ritzwoller, M. H., & Ratnikova, L. I. (1994). The nature and cause of polarization anomalies of surface waves crossing northern and central Eurasia. *Geophysical Journal International*, 117(3), 577–590. <https://doi.org/10.1111/j.1365-246x.1994.tb02455.x>
- Li, J., Beghein, C., Lognonné, P., McLennan, S. M., Wiczeorek, M., Panning, M., et al. (2022). Different Martian crustal seismic velocities across the dichotomy boundary from multi-orbiting surface waves. *Geophysical Research Letters*, 50(1), e2022GL101243. <https://doi.org/10.1029/2022GL101243>
- Li, J., Beghein, C., McLennan, S. M., Horleston, A. C., Charalambous, C., Huang, Q., et al. (2022). Constraints on the Martian crust away from the InSight landing site. *Nature Communications*, 13(1), 1–10. <https://doi.org/10.1038/s41467-022-35662-y>

- Li, J., Beghein, C., Wookey, J., Davis, P., Lognonné, P., Schimmel, M., et al. (2022). Evidence for crustal seismic anisotropy at the InSight lander site. *Earth and Planetary Science Letters*, 593, 117654. <https://doi.org/10.1016/j.epsl.2022.117654>
- Lognonné, P., Banerdt, W. B., Giardini, D., Pike, W. T., Christensen, U., Laudet, P., et al. (2019). SEIS: Insight's seismic experiment for internal structure of Mars. *Space Science Reviews*, 215(1), 1–170. <https://doi.org/10.1007/s11214-018-0574-6>
- Lognonné, P., Banerdt, W. B., Pike, W., Giardini, D., Christensen, U., Garcia, R. F., et al. (2020). Constraints on the shallow elastic and anelastic structure of Mars from InSight seismic data. *Nature Geoscience*, 13(3), 213–220. <https://doi.org/10.1038/s41561-020-0536-y>
- Manga, M., & Wright, V. (2021). No cryosphere-confined aquifer below InSight on Mars. *Geophysical Research Letters*, 48(8), e2021GL093127. <https://doi.org/10.1029/2021gl093127>
- McEvilly, T. (1964). Central US crust—Upper mantle structure from love and Rayleigh wave phase velocity inversion. *Bulletin of the Seismological Society of America*, 54(6A), 1997–2015. <https://doi.org/10.1785/bssa05406a1997>
- Neumann, G. A., Abshire, J. B., Aharonson, O., Garvin, J. B., Sun, X., & Zuber, M. T. (2003). Mars Orbiter Laser Altimeter pulse width measurements and footprint-scale roughness. *Geophysical Research Letters*, 30(11), 1561. <https://doi.org/10.1029/2003gl017048>
- Nimmo, F., & Stevenson, D. (2001). Estimates of Martian crustal thickness from viscous relaxation of topography. *Journal of Geophysical Research*, 106(E3), 5085–5098. <https://doi.org/10.1029/2000je001331>
- Ojha, L., & Lewis, K. (2018). The density of the Medusae Fossae Formation: Implications for its composition, origin, and importance in Martian history. *Journal of Geophysical Research: Planets*, 123(6), 1368–1379. <https://doi.org/10.1029/2018je005565>
- Ondera, K. (2022). Subsurface structure of the Moon and Mars deduced from 3D seismic wave propagation simulation and analysis of Apollo and InSight seismic data. Doctoral dissertation of The Graduate University for Advanced Studies, SOKENDAI and Université de Paris Cité.
- Panning, M. P., Banerdt, W. B., Beghein, C., Carrasco, S., Ceylan, S., Clinton, J. F., et al. (2023). Locating the largest event observed on Mars with multi-orbit surface waves. *Geophysical Research Letters*, 50(1), e2022GL101270. <https://doi.org/10.1029/2022gl101270>
- Posiolova, L., Lognonné, P., Banerdt, W. B., Clinton, J., Collins, G. S., Kawamura, T., et al. (2022). Largest recent impact craters on Mars: Orbital imaging and surface seismic co-investigation. *Science*, 378(6618), 412–417. <https://doi.org/10.1126/science.abq7704>
- Raducan, S., Davison, T., & Collins, G. (2020). The effects of asteroid layering on ejecta mass-velocity distribution and implications for impact momentum transfer. *Planetary and Space Science*, 180, 104756. <https://doi.org/10.1016/j.pss.2019.104756>
- Schimmel, M., Stutzmann, E., Lognonné, P., Compaire, N., Davis, P., Drilleau, M., et al. (2021). Seismic noise autocorrelations on Mars. *Earth and Space Science*, 8(6), e2021EA001755. <https://doi.org/10.1029/2021ea001755>
- Scholz, J.-R., Widmer-Schmidrig, R., Davis, P., Lognonné, P., Pinot, B., Garcia, R. F., et al. (2020). Detection, analysis, and removal of glitches from InSight's seismic data from Mars. *Earth and Space Science*, 7(11), e2020EA001317. <https://doi.org/10.1029/2020ea001317>
- Shapiro, N. M., Ritzwoller, M. H., Molnar, P., & Levin, V. (2004). Thinning and flow of Tibetan crust constrained by seismic anisotropy. *Science*, 305(5681), 233–236. <https://doi.org/10.1126/science.1098276>
- Shapiro, N. M., & Singh, S. (1999). A systematic error in estimating surface-wave group-velocity dispersion curves and a procedure for its correction. *Bulletin of the Seismological Society of America*, 89(4), 1138–1142. <https://doi.org/10.1785/bssa0890041138>
- Shi, J., Plasman, M., Knapmeyer-Endrun, B., Xu, Z., Kawamura, T., Lognonné, P., et al. (2022). High-frequency receiver functions with event S1222a reveal a discontinuity in the Martian shallow crust. *Geophysical Research Letters*, 50(5), e2022GL101627. <https://doi.org/10.1029/2022GL101627>
- Spetzler, J., Trampert, J., & Snieder, R. (2002). The effect of scattering in surface wave tomography. *Geophysical Journal International*, 149(3), 755–767. <https://doi.org/10.1046/j.1365-246x.2002.01683.x>
- Stähler, S. C., Khan, A., Banerdt, W. B., Lognonné, P., Giardini, D., Ceylan, S., et al. (2021). Seismic detection of the Martian core. *Science*, 373(6553), 443–448. <https://doi.org/10.1126/science.abi7730>
- Tanaka, K. L., Skinner, J. A., Jr., Dohm, J. M., Irwin, R. P., III, Kolb, E. J., Fortezzo, C. M., et al. (2014). *Geologic map of Mars*. USGS.
- Wang, N., Montagner, J.-P., Fichtner, A., & Capdeville, Y. (2013). Intrinsic versus extrinsic seismic anisotropy: The radial anisotropy in reference Earth models. *Geophysical Research Letters*, 40(16), 4284–4288. <https://doi.org/10.1002/grl.50873>
- Wieczorek, M. A., Broquet, A., McLennan, S. M., Rivoldini, A., Golombek, M., Antonangeli, D., et al. (2022). InSight constraints on the global character of the Martian crust. *Journal of Geophysical Research: Planets*, 127(5), e2022JE007298. <https://doi.org/10.1029/2022je007298>
- Xu, Z., Broquet, A., Fuji, N., Kawamura, T., Lognonné, P., Montagner, J.-P., et al. (2023). Velocity models from “Investigation of Martian regional crustal structure near the dichotomy using S1222a surface-wave group velocities”. *Zenodo*. <https://doi.org/10.5281/zenodo.7788001>
- Xu, Z., Froment, M., Garcia, R. F., Beucler, É., Ondera, K., Kawamura, T., et al. (2022). Modelling seismic recordings of high-frequency guided infrasound on Mars. *Journal of Geophysical Research: Planets*, 127(11), e2022JE007483. <https://doi.org/10.1029/2022je007483>
- Yoshizawa, K., & Kennett, B. (2005). Sensitivity kernels for finite-frequency surface waves. *Geophysical Journal International*, 162(3), 910–926. <https://doi.org/10.1111/j.1365-246x.2005.02707.x>
- Zhou, Y., Dahlen, F., & Nolet, G. (2004). Three-dimensional sensitivity kernels for surface wave observables. *Geophysical Journal International*, 158(1), 142–168. <https://doi.org/10.1111/j.1365-246x.2004.02324.x>
- Zuber, M. T., Solomon, S. C., Phillips, R. J., Smith, D. E., Tyler, G. L., Aharonson, O., et al. (2000). Internal structure and early thermal evolution of Mars from Mars Global Surveyor topography and gravity. *Science*, 287(5459), 1788–1793. <https://doi.org/10.1126/science.287.5459.1788>